The origin of Fe II and [Fe II] emission lines in the 4,000-10,000 Å range in the BD Weigelt Blobs of Eta Carinae

Verner, E. M.; Gull, T. R.; Bruhweiler, F.; Johansson, Sveneric; Ishibashi, K.; Davidson, K.

Published in:
Astrophysical Journal

DOI:
10.1086/344443

2002

The Astrophysical Journal, 581:1154–1167, 2002 December 20

THE ORIGIN OF Fe II AND [Fe II] EMISSION LINES IN THE 4000–10000 Å RANGE IN THE BD WEIGELT BLOBS OF η CARINAE[1]

E. M. Verner
Catholic University of America and Laboratory of Astronomy and Space Science, NASA Goddard Space Flight Center, Greenbelt, MD 20771; kverner@fe2.gsfc.nasa.gov

T. R. Gull
Laboratory of Astronomy and Space Science, NASA Goddard Space Flight Center, Greenbelt MD 20771; gull@sea.gsfc.nasa.gov

F. Bruhweiler
Catholic University of America and Laboratory of Astronomy and Space Science, NASA Goddard Space Flight Center, Greenbelt, MD 20771; bruhweiler@iacs.gsfc.nasa.gov

S. Johansson
Lund Observatory, Lund University, P.O. Box 43, S-221 00 Lund, Sweden; sveneric.johansson@astro.lu.se

K. Ishibashi
Massachusetts Institute of Technology, Center for Space Research, 77 Massachusetts Avenue, NE80-6011 Cambridge, MA 02139; bish@space.mit.edu

and

K. Davidson
Department of Astronomy, University of Minnesota, Minneapolis, MN 55455; kd@astro.umn.edu
Received 2002 July 30; accepted 2002 August 26

ABSTRACT

We present numerical simulations that reproduce the salient features of the amazingly strong [Fe II] and Fe II emission spectra in the B and D Weigelt blobs of η Carinae. For our studies we have used spectra obtained during the 1998 epoch observations with the *Hubble Space Telescope* (*HST*). The spectrum of the B and D Weigelt blobs dominates in [Fe II] and Fe II emission lines. The same observations show no Fe I or Fe III. We have compared our measurements of the strongest ($\geq$200) [Fe II] and Fe II lines and blends in the spectrum with theoretical predictions. Our predictions are based on non-LTE modeling of the Fe II atom, which includes the lowest 371 energy levels (all levels up to 11.6 eV). We have investigated the dependence of the spectrum on electron density, pumping by the blackbody-like stellar continuum, and intense Lyα emission. We find that radiative pumping is essential in explaining the observed spectrum. We have identified the main pumping routes responsible for the observed Fe II emission. Comparison between the model and observations reveals details of the radiation field. Pumping by the blackbody-like stellar radiation field from η Carinae explains the numerous strong [Fe II] and Fe II lines in the range of 4000–6500 Å. The strongest Fe II lines in a range of 8000–10000 Å are pumped by intense Lyα radiation.

Subject headings: H II regions — ISM: individual (η Carinae) — line: formation — line: identification

On-line material: machine-readable table

1. INTRODUCTION

In 1986, the object known as η Carinae was resolved by speckle interferometry into four components within 0.″3 (Weigelt & Ebersberger 1986). Davidson et al. (1995, 1997) found that the brightest component A is the central star and that the other objects B, C, and D are slow-moving ejecta with extremely unusual emission-line spectra. The size of each blob is comparable to that of our solar system (Davidson & Humphreys 1997). More detailed spectra of the central source, η Carinae, and the BD blobs have been obtained with the Space Telescope Imaging Spectrograph on the *Hubble Space Telescope* (*HST*/STIS) (e.g., Gull, Ishibashi, & Davidson 1999). The radial velocity measurements suggest that they are slow-moving gaseous ejecta with radial velocity ≈ -45 km s^{-1}. The angular distance from the BD blobs to the central stellar source is $\sim$0.″1. Thus, it is large enough to be spatially resolved in *HST*/STIS long-slit spectra. The spectrum of the BD blobs differs from that of the central source. The stellar spectrum is rich in broad H I and Fe II permitted lines (Hiller et al. 2001). In contrast, narrow forbidden Fe II lines dominate in the BD spectrum.

We schematically depict in Figure 1 the position of the STIS long slit relative to that of the BD blobs and the central source (A) in the 1998 observations. We have delineated the outline of the region sampled by the STIS aperture denoted by the bold rectangle. The arrow shows direction and size (9″) to the periphery of the η Carinae Nebula, where the angular scale from the central star to the BD position is much smaller ($\sim$0.″1).

Space *International Ultraviolet Explorer* (*IUE*) and *HST* as well as ground-based observations of the BD blobs show narrow (FWHM $\approx$ 50 km s^{-1}) and strong Fe II and [Fe II]

[1] Based on observations made with the NASA/ESA *Hubble Space Telescope*, obtained at the Space Telescope Science Institute, which is operated by the Association of Universities for Research in Astronomy, Inc., under NASA contract NAS 5-26555.

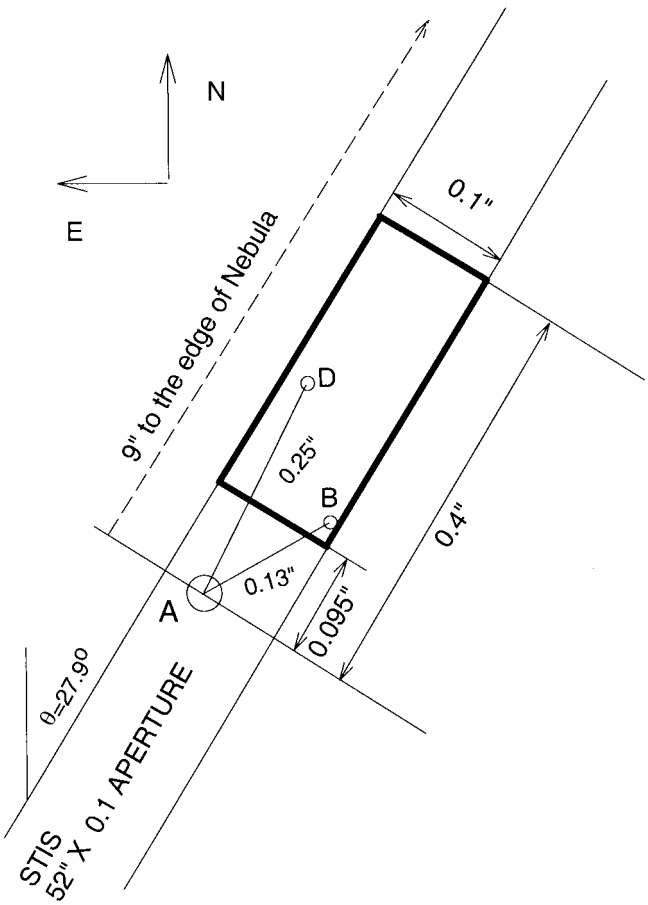

FIG. 1.—Diagram depicting the STIS aperture and placement relative to the η Carinae (A) and the Weigelt blobs B and D. The STIS $52'' \times 0\farcs1$ spectrum was oriented at $-27\fdg9$ position angle. For our modeling we have used only the data reduced for the BD position.

emission lines. Zethson (2001) has identified more than 2500 lines in the BD spectra recorded during 1998, 1999 and 2000 *HST*/STIS observations. These STIS data sets span a 1640–10400 Å spectrum range, with most of the strong [Fe II] and Fe II lines found from 4000 to 10000 Å. Moreover, since there is no Fe I or Fe III emission in the spectrum, the iron must be almost entirely in the form Fe^+.

The most peculiar features are the unusually strong Fe II $\lambda\lambda$2507, 2509 lines identified by Johansson & Jordan (1984). Johansson & Hamann (1993) suggested that a Bowen mechanism produces the unexpected large intensities of these UV lines. Recently, Johansson & Letokhov (2001) considered an excitation mechanism for the 2507 and 2509 Å features based on photoexcitation and photoionization of Fe II by intense Lyα radiation. In their qualitative model, Lyα is generated by the absorption of blackbody radiation from the central star and then trapped within the optically thick environment of the BD blobs.

Previous attempts (Davidson et al. 1997; Hamann et al. 1999) to derive physical conditions in BD blobs were based on an Osterbrock (1989) type line ratio analysis. They deduce electron densities of $n_e = 10^5$–10^{10} cm^{-3}, depending on the ionic diagnostics used. Only a self-consistent quantitative model can provide a more accurate determination of electron density and other physical conditions in the BD blobs.

In this paper, in spite of considerable uncertainties in the atomic data and complexity of physical processes, we present the first quantitative model for the Fe II and [Fe II] emission in the BD knots. We focus on explaining the Fe II and [Fe II] emission spectrum in the wavelength range from 4000 to 10000 Å. Specifically we address the following questions: Why do we see so many strong Fe II and [Fe II] lines? What is temperature and density of the emitting region? What excitation process dominates: collisional excitation, pumping by the incident stellar continuum, or fluorescence by Lyα? Finally, can we explain the Fe II emission by a single density model?

In addition to a complex physical environment, η Carinae also displays dramatic spectral variability. Based on spectroscopic observations of η Carinae with the 1.6 m Laboratorio Nacional de Astrofisica (LNA, Brazil) telescope between 1989 and 1996, Damineli, Conti, & Lopes (1997) have proposed that η Carinae is a stellar binary with a 5.52 yr period. Independent confirmations on the periodicity have come from X-ray observations by Ishibashi et al. (1999) and Pittard & Corcoran (2002). The optical spectrum of the Weigelt blobs mimics this periodicity with the appearance and disappearance of high excitation lines.

The 1998 epoch *HST*/STIS spectra we use here exhibit only low-ionization species. These spectra display no lines of higher ionization like [Ar III], [S III], [Fe III], [Fe IV], and [Ne III] seen in other epochs (e.g., Zethson 2001). As we will show, the general behavior of the Fe II emission lines at optical wavelengths (4000–6500 Å) is mainly due to pumping via the stellar continuum radiation field, while most of strong Fe II emission lines at near-IR wavelengths (8000–10000 Å) are due to the effects of the stellar continuum and intense Lyα radiation. We further employ a previously developed atomic model for Fe II (Verner et al. 1999) to probe the physical conditions in the emitting region where Fe^+ emission originates.

Using the unique spatial and wavelength resolution capabilities of *HST*/STIS, we have performed a detailed study of the Fe II spectrum of the BD knots. This paper presents the first sophisticated numerical model of Fe II emission as a part of fully self-consistent photoionization plasma calculations.

2. THE OBSERVED Fe II SPECTRUM

We have analyzed the highest quality *HST*/STIS spectra of the compact BD ejecta of the η Carinae recorded 1998 March 19 during the 1998 broad spectroscopic minimum (Gull et al. 1999). The spectra were taken with the STIS $52'' \times 0\farcs1$ aperture oriented at a position angle P.A. $= -27\fdg9$ (Fig. 1). Spectral coverage is complete from 1640 to 10600 Å using $\sim$30 grating settings with the CCD and G230MB, G430M, and G750M gratings. The spectral resolving power of the CCD is $R = \lambda/\Delta\lambda \sim$ 5000–10,000. The spatial sampling is $0\farcs0507$ for the STIS/CCD, which corresponds to $\sim 0\farcs10$ at 6500 Å and broadens to $\sim 0\farcs14$ at 10000 Å. While the data resolve the B and D blobs up to 5000 Å, we cannot easily separate the individual spectrum of B from D at longer wavelength, as they are $\sim 0\farcs1$ apart. Therefore, we have extracted a single spectrum for $0\farcs095$ to $0\farcs40$ offset from η Carinae A (see Fig. 1).

The diffracted and scattered light from the central source (component A) of η Carinae primarily contributes to a slowly varying continuum. The Balmer P Cygni profiles are

extended from −1000 to +1000 km s^{-1}, with broad wind absorptions extending to −550 km s^{-1}. Exposure times for each grating setting were chosen to obtain reasonable dynamic range without pixel saturation through the entire wavelength sampled by STIS.

Data reduction and analysis were performed using the IDL CALSTIS software package.[2] It was necessary to disentangle spectra of objects with small angular separation. Thus, the standard STScI pipeline software products were inadequate. The CALSTIS tools available at NASA Goddard Space Flight Center were used to correct for the temporal variations of the optical elements and to linearize the spectral dispersion.

At wavelengths below 3500 Å, both the first-order and echelle spectral modes of the STIS (T. R. Gull et al. 2002, in preparation) demonstrate the presence of complex circumstellar and interstellar absorption along the line of sight to the Weigelt BD blobs. The spectra are dominated by absorption from the ground and low-lying levels of Fe II and other species. These line absorption systems contribute far less longward of 3500 Å. Because of the contamination of these absorptions, we have concentrated on an analysis of the strongest Fe II and [Fe II] emission lines at wavelengths longward of 4000 Å.

3. Fe II LINE IDENTIFICATIONS AND MEASUREMENTS

Preliminary spectroscopic line identification suggested that most of lines/blends in BD blobs are due to singly ionized iron (Zethson 2001). The strongest [Fe II] and Fe II lines are the most prominent candidates to reveal the physical conditions in the gas. Consequently, we have limited the measurements to lines with high signal-to-noise ratio. Our final line identifications are heavily influenced by the results of the model calculations.

Using the energy level data from S. Johansson (2002, private communication), we have identified the relevant Fe II and [Fe II] transitions in the 1998 *HST* spectra. We have adopted atomic data (Quinet, Le Dourneuf, & Zeippen 1996; Zhang & Pradhan 1995; Bautista, Peng, & Pradhan 1996; Kurucz 1981; Nahar 1995; Fuhr, Martin, & Weise 1988) in our modeling. We have compiled a list of the strongest Fe II and [Fe II] lines that are expected to appear in the spectrum of the BD blobs. Based upon this list, we identified more than 200 strong Fe II and [Fe II] lines. For nonblended Fe II lines the heliocentric velocity range is $v_{\odot} = -44 \pm 4$ km s^{-1}. A number of the observed emission features have several possible identifications due to uncertainties in atomic data.

The adopted Fe II ion model includes the lowest 371 energy levels (energies up to 11.6 eV). All the strongest observed lines are produced by transitions within the lowest 344 levels (see Table 1). The upper energy level in the model was chosen to be higher than the highest observed primary cascade produced by Lyα pumping.

Table 1 includes only the strongest [Fe II] and Fe II lines observed in 2000–10000 Å range. Column (1) gives the line identification number (multiple identifications [possible blends] have the same number; column (2) the lists the observed wavelength in the BD rest frame, in Å; column (3) the FWHM; column (4) the observed intensity; column (5) the reddening-corrected intensity; column (6) the multiplet identification, including also information on parity; column (7) the order number of lower level; column (8) the order number of upper level; column (9) the laboratory wavelength, in Å; column (10) the energy of lower level, in cm^{-1}; column (11) energy of upper level, in cm^{-1}; column (12) the statistical weight of lower level; column (13) the statistical weight at upper level; column (14) the transition probability, in s^{-1}; and column (15) the measured line velocity.

We first have attempted to use Fe II line fluxes to determine the extinction correction. However, the emission from many of the lowest states of Fe II is affected by collisional deexcitation. In addition, the strong emission observed from Fe II upper states excited by Lyα pumping shows mixing effects that significantly alter the observed intensities. Finally, there is no Fe II upper level, isolated from mixing, with primary cascades that extend across the wide observed wavelength range. Both collisional deexcitation and mixing negate any attempts to use the Fe II lines to estimate extinction.

Since we found no appropriate Fe II transitions to derive an extinction correction, we used the flux ratios of [S II] $\lambda\lambda$4069, 4079, and 10288. These lines all arise from the same upper level and can provide reasonable extinction estimates. We have adopted the transition probabilities of Pradhan & Peng (1995) in defining our estimates of the reddening. The observed flux ratio of these lines indicates that they have low extinction. The wide wavelength coverage of our data includes [S II] λ10322, but STIS sensitivity drops precipitously at this spectral range. Thus, from the measured [S II] intensities, we derived the corrected intrinsic intensities (I_{λ}) for other lines $I_{\lambda} = k_{\lambda} \times I_{\rm obs}$, where $k_{\lambda} = 8.3 \times 10^{-5}\lambda + 0.63$. In § 4 we show that emission of [S II] and Fe II lines arise in the same emitting region, which demonstrates that the use of [S II] to derive the extinction is relevant.

Since the lines of singly ionized iron are narrow and symmetrical in the BD spectrum, this allowed us to easily fit them with Gaussian profiles and determine the FWHM. The source of errors in the emission-line measurements is more than just statistical. Even for the strongest Fe II lines, where the signal-to-noise ratio is large, significant uncertainties can result from estimating the underlying stellar continuum. Blending of emission lines can also be a contributor. The measured FWHM of the observed [Fe II] and Fe II lines are in a range from 30 to 158 km s^{-1} (Fig. 2). For most of the single lines the FWHM is 50 ± 10 km s^{-1}. Lines with larger FWHM are typically blends. Blends are common because of the richness of the Fe II ionic spectrum as well as that of other ions. For example, the 3259 Å feature with a FWHM = 157.6 km s^{-1} is an example of strong blending. Another example of line overlap is the 9204 Å feature with a FWHM $\sim$ 100 km s^{-1} (Fig. 3). The feature at 9204 Å is resolved and has two peaks at 9203.84 and 9205.32 Å. However, detailed Gaussian fitting suggests that a third Fe II line contributes. The model predictions using CLOUDY indicate that all three lines should be present and are produced by Lyα pumping. More details on these and other line identifications are included in Table 1.

We have selected two spectral regions, one with the weakest ([Fe II] λ5557.844, Fig. 4) and one with the strongest ([Fe II] λ7157, Fig. 5) measured lines as examples of narrow single Fe II lines. Another example that demonstrates unusual physical conditions in the BD blobs is the intensity

[2] CALSTIS Reference Guide (D. Lindler 1999) is available at: http://hires.gsfc.nasa.gov/stis/docs/calstis/calstis.4.html.

TABLE 1

EMISSION-LINE MEASUREMENTS OF STRONGEST Fe^{+} LINES FROM 2000 TO 9800 Å

LID (1)	REST WAVELENGTH (Å) (2)	FWHM (km s^{-1}) (3)	I_{obs} (1.00E+12) (ergs cm^{-2} s^{-1}) (4)	I_{cor} (1.00E+12) (ergs cm^{-2} s^{-1}) (5)	Multiplet (6)	ORDER Lower (7)	ORDER Upper (8)	ID WAVELENGTH (Å) (9)	E_1 (cm^{-1}) (10)	E_u (cm^{-1}) (11)	g_1 (12)	g_u (13)	A_{ul} (s^{-1}) (14)	δV (km s^{-1}) (15)
1.....	2507.152	58.8	8.24	6.91	c^4F–$^6F^o$	98	320	2507.552	50187.817	90067.351	8	10	9.15E + 04	47.9
2.....	2508.678	66.3	8.96	7.51	c^4F–$^4G^o$	98	319	2509.097	50187.817	90042.798	8	10	2.70E + 08	50.0
3.....	2829.075	56.1	1.05	0.91	a^4F–z^6D^o	9	64	2829.534	3117.488	38458.992	4	10		48.7
4.....	2833.469	73.7	2.54	2.20	z^6P^o–e^6D	76	233	2833.918	43238.600	78525.436	6	6	2.70E + 07	
4.....	2833.469	73.7	2.54	2.20	b^4D–y^4H^o	51	180	2834.918	31387.979	66672.335	6	8	3.13E + 03	
5.....	2839.903	58.4	4.54	3.93	z^4F^o–e^4D	78	243	2840.348	44232.537	79439.491	10	8	9.90E + 07	47.0
6.....	2845.881	80.9	5.65	4.89	b^4D–x^4F^o	51	177	2846.219	31387.979	66522.310	6	6	2.93E + 06	
6.....	2845.881	80.9	5.65	4.89	z^4D^o–e^4D	84	245	2846.261	45044.190	80178.002	4	4	5.47E + 07	
6.....	2845.881	80.9	5.65	4.89	z^4F^o–e^4D	80	244	2846.432	44753.814	79885.517	8	6	1.26E + 08	
7.....	3256.360	70.6	3.49	3.14	a^4D–z^6D^o	10	65	3256.827	7955.320	38660.052	8	8	2.50E + 05	43.1

NOTE.—Table 1 is published in its entirety in the electronic edition of the *Astrophysical Journal*. A portion is shown here for guidance regarding its form and content.

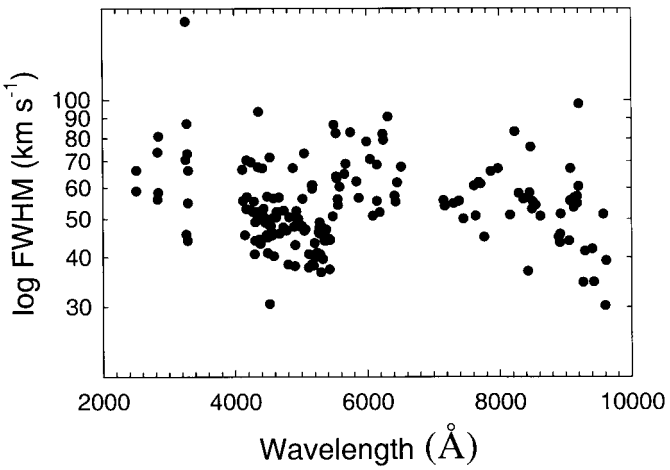

FIG. 2.—Logarithm of measured FWHM of strongest Fe^+ lines plotted against wavelength (Å).

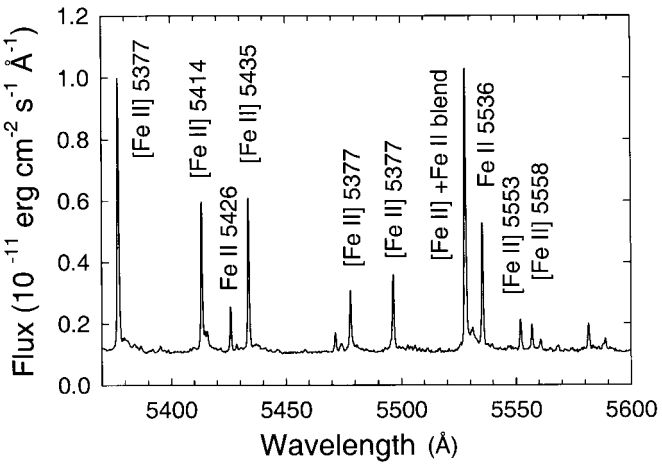

FIG. 4.—Observed *HST* STIS spectrum of the BD blobs showing the weakest measured [Fe II] emission line 5557 Å.

ratio of [N II] λ5755 to [Fe II] λ7157. In an H II region like the Orion Nebula, this ratio is ~20. The depletion of iron in the Orion Nebula is one of factors that make [Fe II] lines weak. η Carinae is known as a nitrogen-rich object, but [Fe II] λ7157 is ~5 stronger than [N II] λ5755 in the BD blobs spectrum. Studies of η Carinae physical conditions (e.g., kinematics, abundances) can provide quantitative information on nebular enrichment and test models of stellar evolution and nucleosynthesis.

Table 1 includes the reddening-corrected [Fe II] and Fe II intensities from 4000 to 10000 Å. After extinction correction, the strongest Fe II line is still the [Fe II] λ7156 ($a^4F_{9/2}$–$a^2G_{9/2}$, Fig. 5). Other strong, but low-excitation, lines are [Fe II] λ5160 ($a^4F_{9/2}$–$a^4H_{13/2}$), and [Fe II] λ4360 ($a\,^6D_{7/2}$–$a\,^6S_{5/2}$). The strongest high-excitation Fe II lines originate in conditions that must include Lyα excitation. The strongest measured line produced by Lyα pumping, and not affected by blending, is Fe II at λ8492 ($e^6D_{5/2}$–$x^6F^o_{7/2}$). However, all the observed lines arise through transitions within the 371 lowest levels.

The UV spectral region from 2000 to 4000 Å of the BD blobs is very difficult to analyze because of complexities in defining the stellar continuum and intervening absorption systems. In Figure 6 the UV emission spectrum of the BD blobs is strongly contaminated by absorption from the ground state and fine-structure levels of the resonance Fe II UV1 multiplet ($\lambda\lambda$2593–2620). This shows that the BD emission is veiled by high column density circumstellar gas along the line of sight. Although we include the measurements of the strongest UV emission Fe II lines in Table 1, the measurements shortward of 4000 Å should be treated with special caution.

4. BASIC PARAMETERS FOR THE MODELING

We need to define the initial parameters for the modeling. As a first step we have searched for the traditional nebular line diagnostics in the spectrum. The FWHM of [S II] λ6731 is twice as large as that of [S II] λ6716. This means that the [S II] λ6731 line must be a blend. The [N II] $\lambda\lambda$3063/5755 line ratio is not reliable because of large UV continuum uncertainties. There is no [O II] emission, and the [O I] line at λ6300 is very weak, while the [O I] λ6363 is not detected. Also, no carbon lines are identified. We find that none of the normal emission-line diagnostics are reliable indicators. Since Fe II and [Fe II] lines dominate the spectrum of the BD

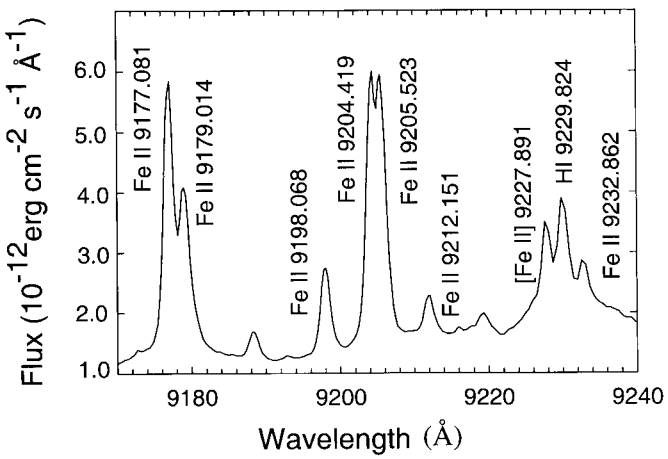

FIG. 3.—9204 Å feature in BD blobs spectrum. It is strongly blended due to Fe II line coincidence. While two peaks are easily seen, the blend includes three Fe II lines, all are due to Lyα pumping.

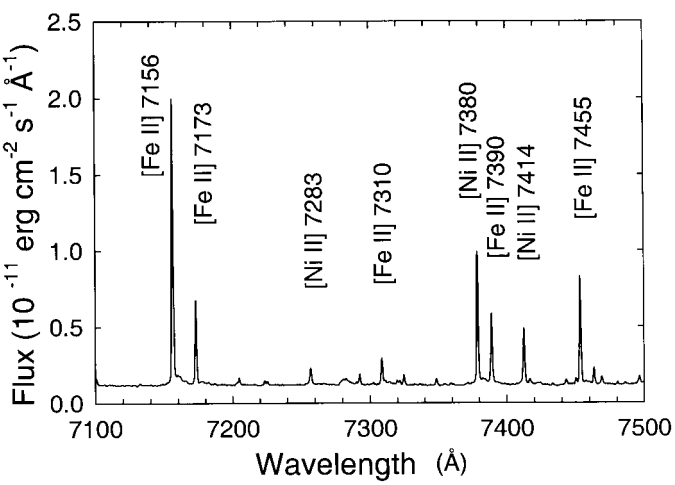

FIG. 5.—Observed *HST* STIS spectrum of the BD blobs showing the strongest measured [Fe II] emission line 7156 Å.

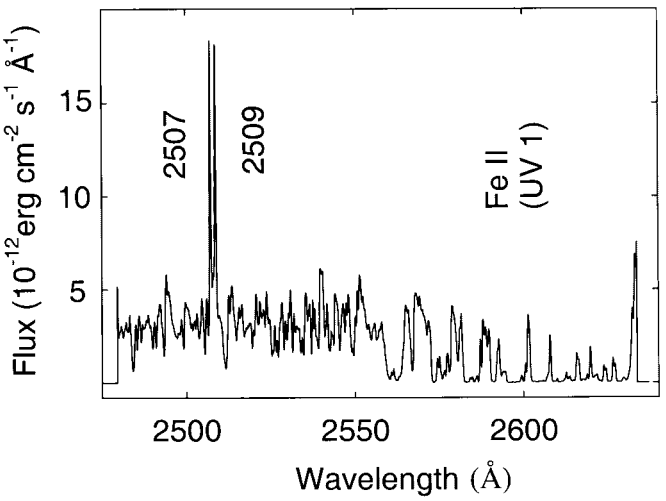

FIG. 6.—BD spectrum in 2480–2650 Å range shows very strong Fe II absorption. Two peculiar Fe II features at 2507 and 2509 Å are also present.

blobs, we cannot avoid them in our modeling. Moreover, failure to use them will certainly lead to the wrong conclusions. Intensities of the strongest and weakest Fe II and [Fe II] lines provide initial clues to the dominant excitation mechanisms and to the range of the electron densities in the Fe^+-emitting plasma. Specifically, the simultaneous presence of strong permitted and forbidden Fe II lines suggests that the electron density range is between 10^4 and 10^7 cm^{-3} (Verner et al. 2000).

The range of physical parameters for numerical modeling is defined using the analysis of Davidson & Humphreys (1997), Davidson (1999), and Hillier et al. (2001). Based on these works, we assume that the total luminosity of central star is $\sim 10^{40}$ ergs s^{-1} and its effective blackbody temperature is in the range $T_{\rm bb} = (1\text{–}3) \times 10^4$ K. The distance from the central star (ionizing source) to the BD blobs is taken to be $R_{\rm BD} = 10^{16}$ cm. The BD blobs have estimated particle densities from 10^5 to 10^{10} cm^{-3}.

Long-term observations of η Carinae (Damineli 1998) and photoionization modeling of the central source (Hillier et al. 2001) support that photoionization and photoexcitation determine the physical conditions in the BD blobs. We have calculated a number of non-LTE models using our atomic model for Fe II and the photoionization code CLOUDY (Ferland 1996; Ferland et al. 1998).[3] To improve upon the Fe II Verner et al. (1999) model, we have upgraded the Fe II energy levels, and include the effects of mixing for the most important levels that are closely spaced in energy (Johansson 1984). To make Lyα pumping effectively work at every pumping channel, we have dramatically increased the number of frequency points defining the Lyα radiation. It is now possible using a new option in CLOUDY to obtain finer energy spacing to adequately describe the radiation field.

The effects of dust are highly variable along different lines of sight toward η Carinae and to its surrounding nebulosity, the Homunculus (Davidson et al. 1995; Hillier et al. 2001). The dust scattering is much stronger in the direction to the central source than in the direction to the BD blobs. Although we have corrected the Fe II intensities for dust extinction before initiating our modeling, we do not investigate the details. Davidson et al. (1995) previously noted the possibility of gray dust in the BD direction. If it were included in models, it would cause significant Fe II line enhancement in the near-IR range relative to that at shorter wavelengths, which is not observed. We have not included dust in our subsequent modeling.

[3] See http://www.pa.uky.edu/~gary/cloudy.

5. THE PHYSICAL CONDITIONS IN THE Fe II EMITTING REGION OF THE BD BLOBS

In recent years, great strides have been made in interpreting the observed η Carinae spectroscopic events (Damineli 1997; Davidson & Humphreys 1997) and a large amount of data have been obtained using *HST*/STIS (Gull et al. 1999, 2001). Still, there is no quantitative model that explains why the BD spectrum in 1998 observations is dominated by lines almost solely from singly ionized iron-group elements.

It is not a typical situation when iron emits only in Fe II and when Fe II are also the strongest lines in the spectrum. For example, in H II regions like the Orion Nebula, [Fe III], as well as [Fe II] emission (Baldwin et al. 2000), is present. Why did we not see any sign of Fe I or Fe III lines in the 1998 observations? Why is the Fe II spectrum so strong and rich in the BD blobs? Is it an excitation or abundance effect? How dense is the material of the Fe^+ emitting region? Why do we see so many lines from metals (like Ni II, Cr II, etc.)? In this section we present our photoionization model of the emitting region in the BD blobs. Our approach predicts the ionization structure of all elements, electron density, and temperature. It also determines the dominant coolant in the emitting plasma.

We have done the photoionization calculations over the range of possible electron densities to investigate how the ionization structure changes. We further adopt a blackbody temperature $T_{\rm BB} = 15,000$ K (see § 7 for more details). Figure 7 presents model results for the expected range of electron densities for η Carinae in the vicinity of the BD blobs. Each plotted value denotes the electron density and corresponding distance from central source to the BD position where the Fe^+/Fe ionization fraction reaches 97%. The dashed line depicts $R_{\rm BD} = 10^{16}$ cm for the distance of the BD blobs from the central source. The distance $R_{\rm BD} \sim 10^{16.3}$ cm (Davidson & Humphreys 1997) is even more consistent with an electron density of 10^6 cm^{-3} for the Fe^+ emitting region.

If electron density ranges from 10^5 to 10^7 cm^{-3}, at least 97% of the atomic iron exists in Fe^+. If the emitting gas has n_e within this range, it could easily explain the unusual Fe^+/Fe ionization in the BD blobs during the 1998 epoch. As seen from Figure 7, the model with $n_e = 10^5$ cm^{-3} predicts the Fe^{+2}/Fe^+ transition at a larger distance ($R_{\rm BD} > 3 \times 10^{17}$ cm) than assumed for the distance of BD blobs from the central ionizing source. If the electron density is near its upper allowed limit (10^7 cm^{-3}), then the range of distance where Fe^+ ionization fraction dominates over Fe^{2+} is much closer to the central source than the expected BD position. Assuming constant density, we find $n_e = 10^6$ cm^{-3} best provides the required dominant Fe^+ fraction for acceptable distances of the BD blobs.

The model predicts an extremely sharp ionization transition between Fe^+ and Fe^{2+} ionization fractions, with little

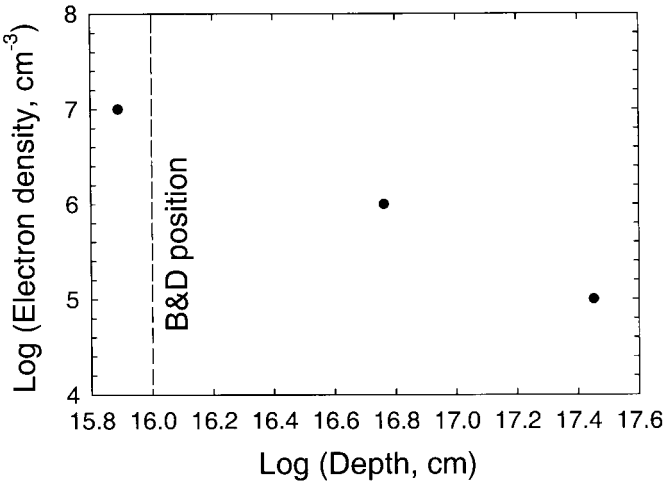

FIG. 7.—Model predictions of the distance for η Carinae where 97% of iron is in Fe^+, for electron densities of 10^5, 10^6, and 10^7 cm^{-3}. The dashed line indicates the position of BD blobs. If the BD blobs electron density is 10^7 cm^{-3}, then the neutral iron is dominant form. With the density of 10^5 cm^{-3}, the iron in BD blobs is in a form of Fe^{2+}. The most probable electron density is $\sim 10^6$ cm^{-3}.

overlap at any electron density. A sharp ionization transition is typical for collisionally ionized plasma (Verner & Yakovlev 1990). Figure 8 shows the Fe^+ and Fe^{2+} ionization structure calculated for a typical model of the BD blobs with electron density 10^6 cm^{-3}. With an electron density range of 10^5 to 10^7 cm^{-3}, the predicted total hydrogen column densities are large, varying from 3×10^{22} to 4.5×10^{23} cm^{-2}. The corresponding logarithm of ionization parameter, $\log U(\mathrm{H}) = \log[\Phi/(n_{\mathrm{H}}c)]$ in our model varies from 0 to -2, where Φ is the total flux of hydrogen ionizing photons at the illuminated face, n_{H} is the hydrogen number density, and c is a speed of light.

The Fe^+ ion is the most important coolant in the BD blobs and carries up to 85% of the total cooling (Fig. 9). Figures 9 and 10 show changes in Fe II cooling (relative to total cooling) and changes in the electron temperature with increasing cloud depth. As the distance from the central source increases, the temperature slightly decreases, and the

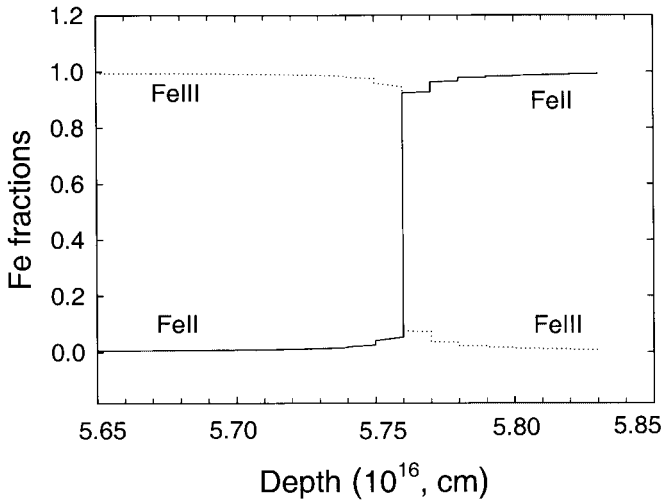

FIG. 8.—Ionization fractions of Fe^+ and Fe^{2+} vs. depth within the cloud (cm). Sharp ionization front for Fe II and Fe III is presented.

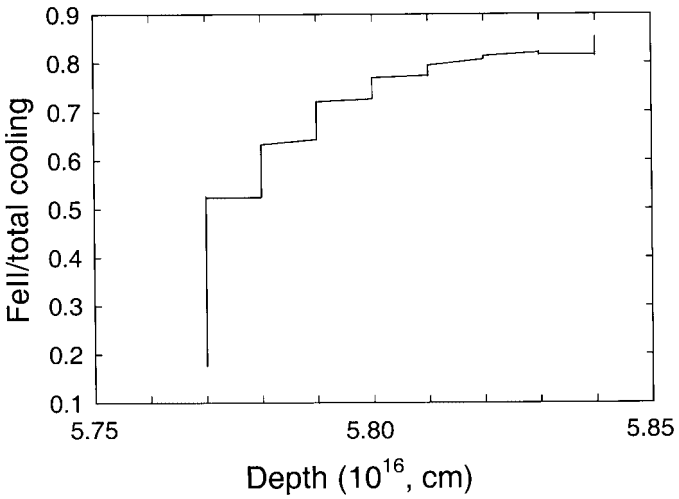

FIG. 9.—Model-predicted fractional cooling of Fe II relative to total cooling rate vs. depth within the cloud (cm).

Fe^{2+} recombines to yield Fe^+. When the ionization fraction of Fe^+ reaches 0.1, Fe II and [Fe II] start to dominate the emission. Then the temperature drops even faster, further increasing Fe^+. This Fe^+ cooling also causes all other ions to recombine to lower ionization stages. Our modeling of the BD blobs indicates that the Fe II emission originates at electron temperatures, 5000 K $\leq T_e \leq$ 7500 K at distance $\sim 5.76 \times 10^{16}$ cm from central source. The derived size of Fe^+ emitting zone (Fig. 8) is $\sim$10 times smaller ($\approx 10^{15}$ cm) than the distance to the BD blobs and agrees with the value derived by Davidson & Humphreys (1997).

The ionization transition for H^+/H^0 is not as sharp as that for Fe^{2+}/Fe^+ in the BD blobs. Within the Fe II emitting region, hydrogen is significantly ionized. At the position of the Fe^{2+}/Fe^+ transition, the ionization fraction of hydrogen is $\sim$0.5. Then at lower temperature, the H^+ gradually recombines to yield H^0 (Fig. 11). Thus, the Fe II emission originates in a region where hydrogen is partially ionized. This also explains why the Fe II and H I lines are represented by very different spectral line shapes in BD blobs, since their emitting regions do not coincide.

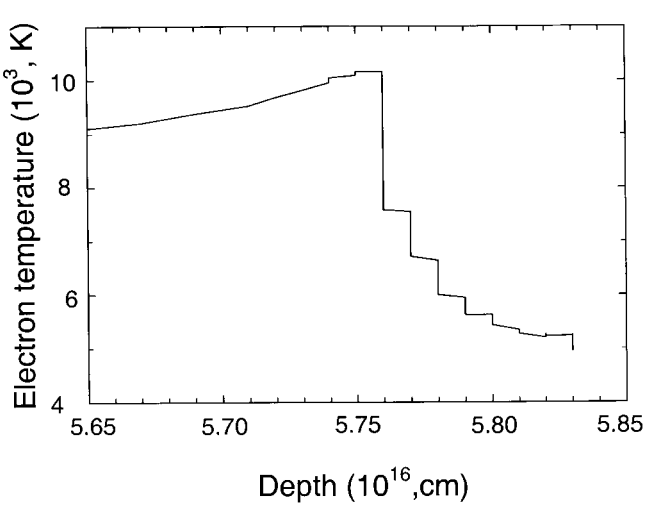

FIG. 10.—Electron temperature (K) vs. depth within the cloud (cm) in the direction from η Carinae.

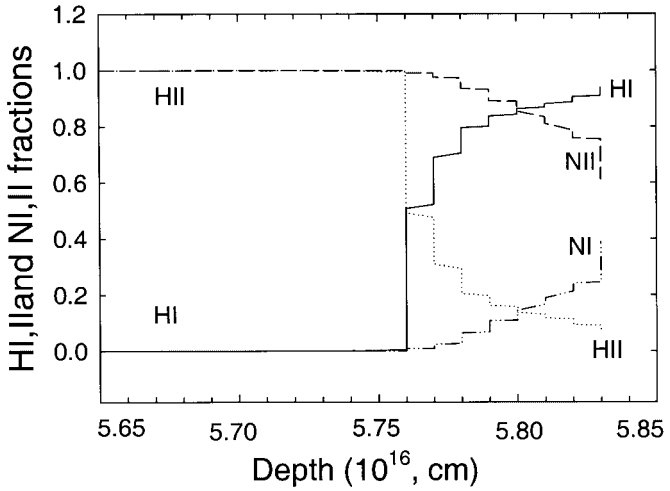

FIG. 11.—Ionization fractions of H^0, H^+ and of N^0, N^+ vs. depth within the cloud (cm). The ionization fronts are not sharp. A significant portion of the Fe II emission comes from partly ionized region.

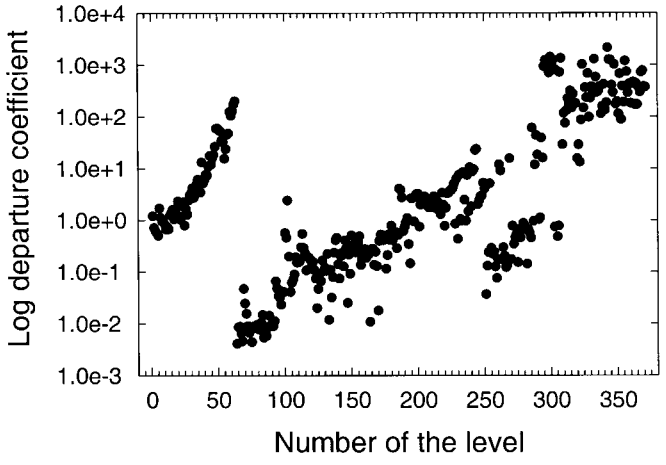

FIG. 13.—Log of the departure coefficient for each Fe II level for the BD blob model, which includes collisional, continuum, and Lyα pumping. Effective cascades from first available odd parity levels make these levels underpopulated.

Figure 12 shows the relative fractions of Fe^+ and Fe^{2+}, and fractions of other ions (N^0, N^+, S^+, and Cr^+) into the depth of cloud. Nitrogen has the ionization potential similar to H I and like hydrogen is partly ionized within the Fe^+ emitting region. Thus, the simultaneous presence of permitted N I and forbidden N II lines indicates that N^0 and N^+ are formed in the same region as Fe^+ in the B and D blobs in the 1998 spectra and supports the photoionization model.

6. ARE NLTE EFFECTS IMPORTANT?

Is it possible to apply a simple local thermodynamic equilibrium (LTE) approach to explain Fe II emission spectrum in BD blobs? We have previously verified that our model goes to LTE conditions (Verner et al. 1999) in four limiting cases: collision-dominated, radiative dominated, large optical depths, and thermal equilibrium. These tests also show that the Fe II multiple energy structure makes the ion very sensitive to collisions, continuum pumping, and line pumping. The lower and upper levels of the Fe II ion approach LTE at different electron densities. For example, the level populations of the entire atom approaches LTE in the collision-dominated case at densities $n_e > 10^{16}$ cm^{-3}. Meanwhile, the lowest Fe II levels, at energies $E \leq 2.3$ eV, reach LTE at $n_e > 10^8$ cm^{-3}. For comparison, the BD blob's spectrum clearly shows the presence of Fe II lines originating from levels up to 11 eV. Thus, in order to adequately populate these higher energy levels, we must have either high collisional excitation (high n_e) or high radiation excitation (strong radiation field).

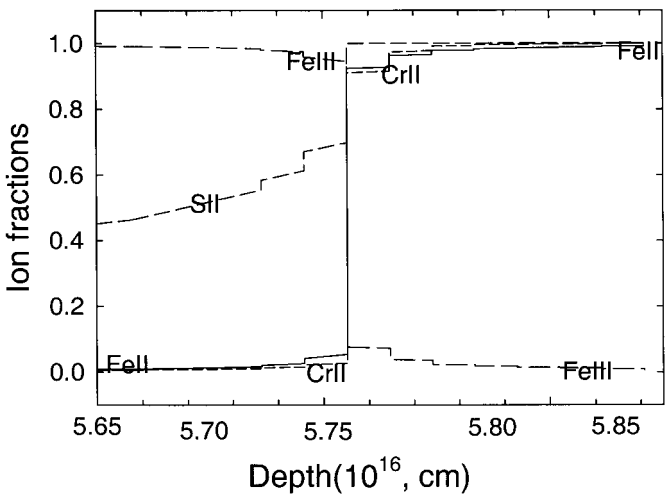

FIG. 12.—Same as Fig. 11, but Cr^+ and S^+ ionization fractions are added for comparison. Ionization fronts are also very sharp and occur at the same depth as for Fe^+.

To evaluate the conditions in BD blobs, we have used departure coefficients, $b_i = n_i/n_{i,\mathrm{LTE}}$, where n_i is the population of ith level and $n_{i,\mathrm{LTE}}$ is that given by LTE from Boltzmann distribution. Figure 13 shows departure coefficients of each level in our model. The full model calculations for an electron density $n_e = 10^{16}$ cm^{-3} confirm that most of the high Fe II energy levels are far from LTE, while the lowest 27 level populations ($E_i \leq 2.3$ eV) are near LTE, with b_i approaching unity. The high optical depth in the BD blobs reduces the radiative rates and allows the lowest levels to approach LTE conditions. The absorption goes effectively from the first odd parity level (i.e., 64 in our model, $\sim$4.8 eV) to these lowest levels. Consequently, the absorption in Fe II can occur up to 3970.50 Å in BD conditions. The most significant departure from LTE in level population is at 64th level. This is first odd parity level, so the first permitted transition is possible from this level.

Figure 13 also illustrates that upper Fe II levels are effectively pumped by blackbody radiation. The departure coefficients of the levels pumped by Lyα (in the range $\sim$89890–89925 cm^{-1}, or 11–11.31 eV) are smaller than those pumped by continuum radiation. (Note that 1 eV = 8065.53851 cm^{-1}.)

7. EFFECT OF BLACKBODY PUMPING ON Fe II EMISSION IN BD BLOBS

η Carinae is extremely luminous, but the exact nature of the central object is not yet resolved. If one represents the radiation field by a blackbody, then spectroscopic studies suggest a wide range for the blackbody temperature.

Davidson et al. (1995) advocated that the UV–visual energy distribution corresponds to a range of blackbody temperature from 20,000 to 30,000 K. Based on *HST*/GHRS spectra analysis at wavelengths less than 1765 Å, Ebbets, Walborn, & Parker (1997) concluded that the stellar wind is similar to a B-type supergiant with a temperature range from 13,000 to 30,000 K.

In our calculations we have included continuum pumping from the central source of η Carinae, approximated with the shape of a diluted blackbody radiation field. The initial range of the blackbody temperature is varied from 10,000 to 30,000 K. We find that the line fluxes and wavelength distribution of predicted observable Fe II transitions change dramatically depending on the electron density and blackbody temperature. The best fit between the model and the observed spectrum is achieved at blackbody temperature $T_{\rm BB} \sim 15{,}000 \pm 2000$ K.

Hillier et al. (2001) compared the spectrum of the η Carinae central source with the P Cygni star HDE 316285. One of the most remarkable spectroscopic similarities between η Carinae and HDE 316285 is the Fe II stellar spectrum. The only major difference is the Fe II λ6489 feature, which is much weaker in η Carinae. The spectral variability, stellar properties, and chemical composition of HDE 316285 is typical of luminous blue variables (LBVs). Our derived blackbody temperature $T_{\rm BB} \sim 15{,}000$ K for the radiation field of the BD blobs is similar to effective temperature of HDE 316285 (Hillier et al. 1998). At this temperature the radiation field effectively pumps a large number of Fe II levels from 912 to 10000 Å.

In a previous study of continuum pumping, Verner et al. (2000) identified important routes for exciting the observed [Fe II] lines in the Orion Nebula. Lower effective temperature and higher densities make continuum pumping even more effective in the BD blobs. Collisional excitation more effectively populates the lower levels at higher densities to make them "launching pads" for continuum pumping. A lower temperature provides a flatter spectral energy distribution for the continuum, which is more effective in pumping over a wider range of wavelengths. The detailed Fe II analysis shows that the strong pumping routes arise from the a^4D and a^2G terms. The excited electrons in these levels then cascade down through intermediate levels, emitting visible photons.

We have evaluated changes in the Fe II emission spectrum by varying the electron density and blackbody temperature. We suggest three spectral ranges with various degree of sensitivity to electron density and blackbody temperature:

1. The 4000–6000 Å range contains most of the prominent Fe II and [Fe II] features. The upper levels for observed transitions are clustered near 2 eV (forbidden lines) and near 6 eV (permitted lines). The unique fit for these lines is achieved at $T_{\rm BB} = 15{,}000$ K and $n_e = 10^6$ cm^{-3}. The evidence to support the presence of a strong blackbody radiation field is the number of strong permitted lines (e.g., a^6S–z^6P^o multiplet) reproduced only in models with continuum pumping.

2. The 6000–6500 Å range contains ~15 permitted lines. Their intensities are smaller than that of lines predominantly in the 4000–6000 Å range. These lines arise due to transitions between levels 4–6 eV above ground (multiplets a^4G–z^6F^o, b^4D–z^4P^o, z^4D^o–c^4D, and a^6S–z^6D^o). Their predicted intensities are slightly underestimated at $T_{\rm BB} = 15{,}000$ K and $n_e = 10^6$ cm^{-3}. The model predicts these lines become unobservable at $n_e < 10^6$ cm^{-3} at any blackbody temperature. Their predicted intensities are too strong compared to observations at $n_e \geq 10^7$ cm^{-3} at blackbody temperatures $\leq$10,000 K. Since there are no collisional excitation rates yet available for these transitions, we estimate them using the g-bar approximation (Mewe 1972).

3. The 7000–9300 Å range contains a few forbidden lines (multiplets a^4F–a^4P and a^4F–a^2G). Their upper levels are $\leq$2 eV above ground. For densities suitable for 1 and 2 above, the [Fe II] λ7156 line is predicted to have an intensity half that observed. Possibly, regions with electron densities $n_e \leq 10^5$ cm^{-3} contribute to this line. Models with blackbody temperatures $\leq$10,000 K do not predict this line well at any density. A change of $T_{\rm BB} = 15{,}000$–$20{,}000$ K does not appreciably affect the predicted intensity.

We have used the "default CLOUDY" version to predict Fe II spectrum ("model A3"). This version is included the standard set of Fe II atomic data and excitation conditions. Excitation conditions are determined by collisions, continuum pumping, and pumping by nebulae Lyα radiation. We have found the best single density model (Fig. 14) at $n_e = 10^6$ cm^{-3} and $T_{\rm BB} = 15{,}000$ K. This model also predicts that iron is mainly in the form of Fe^+.

The blackbody radiation field and Lyα pumping compete with collisional excitation to redistribute the level populations in Fe^+ and greatly affect the Fe II spectrum over the whole observed spectral range throughout the range of parameters 10^5 cm$^{-3} \leq n_e \leq 10^7$ cm^{-3} and $15{,}000$ K $\leq T_{\rm BB} \leq 30{,}000$ K. We have studied the contribution of various excitation mechanisms (collisions, continuum pumping, and Lyα pumping) to the predicted Fe II spectrum. We have computed a series of models by disabling one of these excitation mechanisms. By doing so we explore the importance of this mechanism in explaining the richness of Fe II spectrum. Figure 14 depicts model A, assuming the following subsets of excitation conditions:

A1. *Collisions and* Lyα *pumping*.—This model does not include Fe II pumping by blackbody radiation (Fig. 14, *upper panel*). The [Fe II] λ7156 feature becomes strong for $n_e \geq 10^5$ cm^{-3} and $T_{\rm BB} \geq 15{,}000$ K. The predicted Fe II intensities are too weak compared to the complete model (see model A3). To explain the strength of Fe II emission, the iron abundance must be 50–80 times larger than in the model with continuum pumping (model A2) and the model with both continuum and Lyα pumping (model A3). Moreover, lines from multiplets a^6S–z^6P^o, a^4G–z^6F^o, b^4D–z^4P^o, z^4D^o–c^4D, and a^6S–z^6D^o are not predicted at any density. Effects of Lyα pumping are so small that the strongest predicted lines in the near IR are due to collisions from the ground (the 17th lowest Fe II levels with energy up to 2 eV). Since the collisions at $n_e = 10^5$–10^7 cm^{-3} do not sufficiently populate the upper levels of Fe II pumping channels, the effects of Lyα pumping are negligible. This model also does not reproduce the observed strong, rich spectrum in the 5000–6500 Å range.

A2. *Collisions and continuum pumping*.—This model does not include Fe II pumping by Lyα radiation. The strengths of Fe II lines are dramatically increased when blackbody radiation is included. Lines from a^6S–z^6P^o, a^4G–z^6F^o, b^4D–z^4P^o, z^4D^o–c^4D, and a^6S–z^6D^o multiplets are predicted. Comparison with model A1 shows that not only

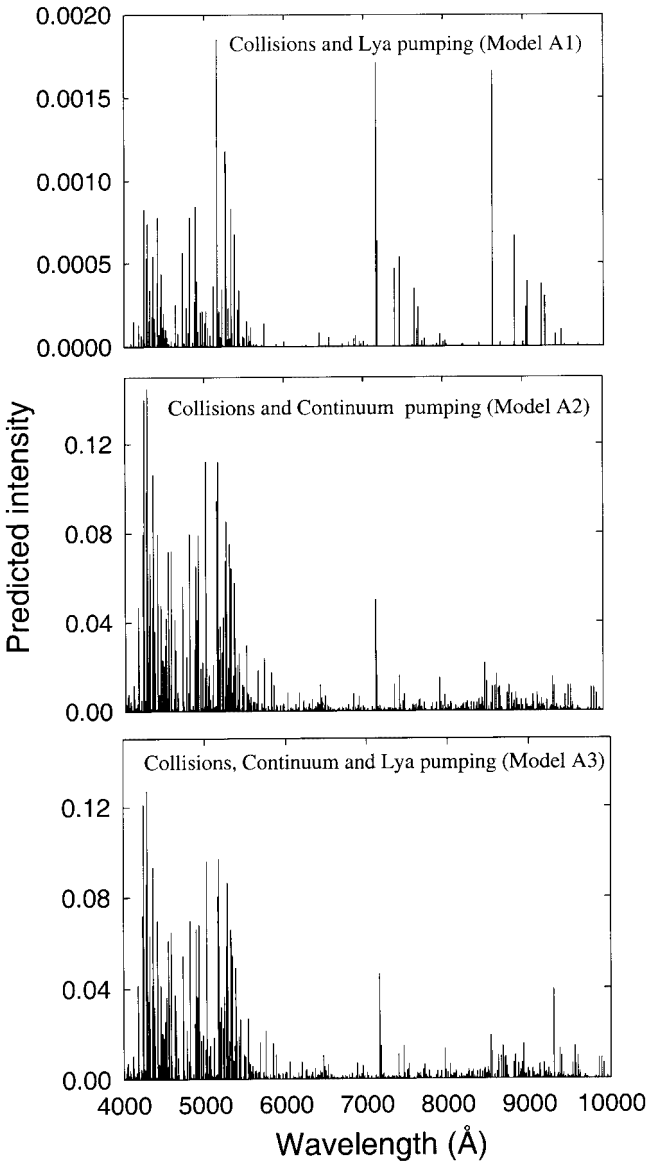

FIG. 14.—Fe II intensities predicted at various excitation conditions $n_e = 10^6$ cm^{-3} and $T_{BB} = 15{,}000$ K. The total luminosity is 10^{40} ergs s^{-1}, and the distance to BD blobs from central star is 10^{16} cm. See text for details of models A1, A2, and A3.

permitted lines, but also low-lying forbidden transitions, are strongly affected by continuum radiation.

A3. *Collisions, continuum, and* Lyα *pumping*.—This model includes all excitation processes. The presence of Lyα pumping helps explain the strength and appearance of lines from a^4F–a^4P and z^6D^o–c^4P multiplets with upper levels below 1.7 eV and 6.2 eV, respectively. The complete model is able to predict only some Fe II primary cascades due to Lyα pumping, the strongest being Fe II λ9299 (e^4D–$^4D^o$). The other Fe II intensities from primary cascades are at least 10 times smaller than seen in observations. We provide more details about Lyα pumping and show how our model can be improved in the next section.

A comparison of models A1, A2, and A3 shows that the continuum radiation field from the central source plays the dominant role in producing the strong, rich Fe II spectrum in the 4000–6500 Å range. Its presence is also important for reproducing the observed strengths of predominantly collisionally excited and Lyα-pumped lines.

8. EFFECT OF Lyα PUMPING ON Fe II EMISSION IN THE BD BLOBS

In this section we discuss the details of Lyα pumping fluorescence. Using existing A values we analyze the branching ratios for pumping routes and primary cascades due to Lyα fluorescence. We compare the results from different models: model A (specifically A3) includes Lyα radiation based on predictions from the photoionization CLOUDY code, and model B assumes very intense Lyα radiation with the Lyα width of 10 Å. Model C is the same as model B, except with different atomic data.

8.1. Lyα *Excitation Routes and Primary Cascades*

Generally in Fe II, the higher the energy level, the closer they are spaced in energy. Because of this close energy spacing, a number of upper levels can be populated via photoexcitation by Lyα emission. These levels then effectively produce cascades with strong emission lines observed in spectra. It is also possible that only one Fe II level in an *LS* term gets pumped, which will cause a huge departure in intensities compare to branching ratios.

We have found that 24 Fe II lines and blends in the ~8000–9600 Å range are primary cascades due to Lyα pumping in the BD blobs. However, only two others are strong in the UV, namely, Fe II λ2507 and λ2509. Because of wavelength coincidence, the most "effective" term for Lyα pumping is the a^4D term.

Table 2 presents details about the most important Fe II pumping channels due to Lyα coincidence and the strongest Fe II primary cascades. This information is based on radiative values used in model A3 and *HST* data. Table 2 has two main parts. The left side includes information about the main pumping routes and about the lower level from which electrons are radiatively pumped; the larger the A value, the larger the radiative rate. Each electron that is pumped to the upper level will cascade according to the branching ratios. The strengths of the lines are in proportion to the branching ratios (if the upper level is the same). The right side of Table 2 provides information on the strongest primary cascades. Column (1) lists the Fe II upper level in the transition pumped by Lyα fluorescence; column (2) the wavelength of Fe II pumped channel, in Å; column (3) the Fe II lower level in transition pumped by Lyα fluorescence; column (4) the transition probability, in s^{-1}, for the pumped transition; column (5) the wavelength of Fe II primary cascade, in Å; column (6) the Fe II lower level in primary cascade; column (7) the branching ratio (in decreasing order) for given upper Fe II level; and column (8) gives notes. The Fe II λ2507 and 2509 features exhibit unusual behavior that has been already discussed in previous studies (cf. Johansson & Letokhov 2001). Specifically, these two transitions have very small A values for any pumping route or primary cascade, yet they are among the strongest observable Fe II lines.

Since many Fe II lines overlap, it is important to ascertain the strongest single Fe II line pumped by Lyα. First, it will provide information about the wavelength of the most effective Fe II pumping channel. Combined information about pumping channels provides an estimate of the width of Lyα. Second, its intensity can be used for reliable comparison

TABLE 2

Lyα Pumping Channels of Most Important Primary Cascades in Fe^+ Ion for the Conditions of BD Blobs in η Carinae (1998)

	Pumping Channel			Primary Cascades			
Pumped Level (1)	λ_{pump} (Å) (2)	Lower Level (3)	A_{ul} (s^{-1}) (4)	λ_{cas} (Å) (5)	Lower Level (6)	Branching Ratios (7)	Notes (8)
319	1218.213	10	1.41E+02	2509.097	98	0.43	Peculiar
				1457.462	27	0.34	Not possible to observe in current observations
				1487.377	33	0.11	Not possible to observe in current observations
				8470.919	231	$<10^{-3}$	Blend with 8471.041 Å line
320	1217.848	10	2.43E+06	8453.337	231	0.43	Single observed line
				9409.232	243	0.13	Single observed line
				8192.888	228	0.11	Not seen in observations
				2507.552	98	10^{-3}	Peculiar
322	1214.398	10	2.28E+06				
	1220.872	11	2.74E+07	8492.435	233	0.22	Single observed line
				1220.872	11	0.21	Not possible to observe in current observations
				8289.869	231	0.12	Blend with 8289.757 Å and 8290.155 Å
				1138.039	7	0.09	Not possible to observe in current observations
				9207.145	243	0.07	Blend with 9205.701 Å and 9206.622 Å
				9601.440	244	0.06	Possible blend with 9601.075 Å

between model and observations. Figure 15 shows the dereddened measured intensities versus pumped upper level from our model. Filled circles are used for intensities of the single pumped lines. Open circles are used for intensities of blended features. All primary cascades originate from levels that are in a range of ~11–11.3 eV. The strongest feature at λ9204 is a blend of three lines pumped by Lyα. The strongest measured intensity of the single line at λ8491 is due to the primary cascade that corresponds to 322th level (≈11.2 eV). The lower limit of Lyα at ~1212 Å and the upper limit of Lyα at ~1222 Å are determined to make pumping channels effectively work for all observed Fe II primary cascades (see Table 1).

In the previous section we have mentioned that the complete model with Lyα pumping (model A3; Fig. 14) predicts Fe II primary cascades, yet not all of them. To understand why, we have compared observable Fe II primary cascades with that predicted from model A.

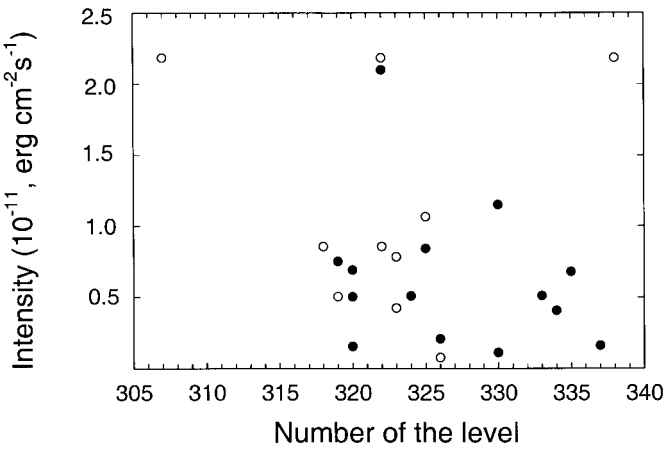

Fig. 15.—Fe II upper levels that are pumped by Lyα excitation and their intensities due to primary cascades. Open circles indicate intensities for blended lines. Filled circles are for single lines. The strongest measured single line originates from 322d level in the Fe II ion. The strongest blended feature (near 9204 Å) is due to cascades from the 322, 338, and 307 levels.

8.2. Lyα *Fluorescence, Model A*

We have found (§ 7) that model A3, when Lyα radiation is predicted from CLOUDY calculations, does not reproduce the strongest observable Fe II primary cascades. For a range of electron densities 10^5–10^7 cm^{-3}, CLOUDY predicts Lyα much narrower (~5 Å) and weaker than required to explain the Fe II primary cascades in BD blobs. With such a narrow-line profile, the Lyα intensity in model vanishes longward to ~1218 Å. This wavelength corresponds to the most effective pumping channel for the peculiar 2507 and 2509 Å features, and observed 8453 Å line (see also Table 2). Since the Lyα flux falls off dramatically at ~1218 Å, the predicted number of Fe II primary cascades is less than observed. Figure 14 (*lower panel*) shows the Fe II intensities predicted by model A.

Model A uses Lyα intensity and width predicted for the local nebular conditions. We have to introduce the intense Lyα radiation (model B) to check whether the model with constant density 10^6 cm^{-3} is able to explain observed Fe II primary cascades.

8.3. Lyα *Fluorescence, Model B*

Keeping all parameters in the model B the same as in model A, we have intentionally modified the shape of the Lyα intensity in the stellar radiation continuum. First, the total Lyα flux has been increased to reproduce the strongest Fe II primary cascades. Second, for simplicity, we have used a Lyα rectangular shaped profile. Evaluating pumping channels and wavelengths of primary cascades, we estimate that the Lyα width must be at least ≈10 Å. The width of Lyα was changed to provide observed intensities consistent with observations on primary cascades of the pumped Fe II levels. Stellar atmosphere modeling done by J. Hillier (2001; and private communication) indicates that up to 50% of total the radiation may come from Lyα. Furthermore, Johansson & Letokhov (2001) have also suggested an intense Lyα radiation field to explain the strength of the peculiar features at 2507 and 2509 Å.

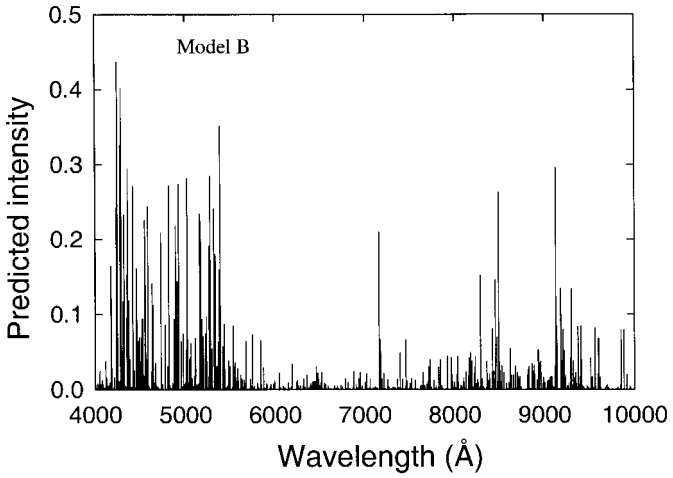

FIG. 16.—Same as Fig. 14, but with intense Lyα pumping model B

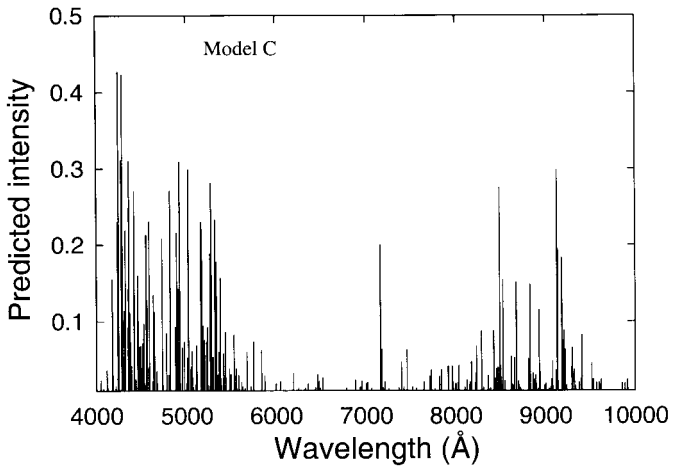

FIG. 17.—Same as in Fig. 16, but with modified atomic data model C

Model B predicts the strongest observable line for each multiplet accordingly used branching ratios (e.g., 8453 Å line in Table 2). There are a few cases in which the atomic data simply are not in agreement with observations. The Fe II $\lambda\lambda$2509 and 2509 lines are most noteworthy (Table 2). The A value of 2509 Å feature is small in our original model. It is not clear how the line could be strong even if its branching ratio is the largest from this level. On the other hand, the upper level of 2507 Å line should be strongly pumped by Lyα due to coincidence because of a large A value. But the corresponding branching ratio is too small to explain the strength of the observed line.

Figure 16 shows model B. The main difference between model A and model B is the presence of strong Fe II primary cascades pumped by Lyα. The presence of intense Lyα line (model B) does not explain the strength of famous 2507 and 2509 Å features. In model B they are too weak at any of the physical parameters: Lyα intensity, density, strength of radiation field, and $T_{\rm BB}$. It is important to explain the origin of these lines because they are observed in other objects (e.g., in RR Telescopii; see Hartman & Johansson 2000).

8.4. Lyα *Fluorescence, Model C*

Because of a high level density of upper Fe II states, the level mixing causes changes in the A values. It is difficult to predict A values theoretically. In an attempt to improve the A values, we have changed them from theoretical values (Nahar 1995) to the A vales of the Kurucz database (1983), where experimental A values have been inserted when available.

To solve the problem of the 2507 and 2509 Å features, we have implemented mixing for their upper levels ($^6F^o_{9/2}$ and $^4G^o_{9/2}$), which are very close in energy ($\approx$25 cm^{-1}). We have adopted 50% for the mixing of these levels, as suggested by Johansson (1984). Two upper levels are treated as a combination of two different states. They are pumped with 50% of the most effective route and cascade with 50% of the most effective primary cascade.

Model C successfully predict Fe II 2507 and 2509 Å lines as the strongest lines in the whole spectrum. However, a number of lines in near IR from 8000 Å to 10000 Å are larger than observed (Fig. 17).

8.5. *Comments on* Lyα *Fluorescence Modeling*

The *HST* observations of η Carinae nebula show a broad absorption in Lyα. The interstellar circumstellar absorption completely scatters any intrinsic stellar emission. Thus, there is no information on the intrinsic stellar Lyα emission profile. The simple photoionization model that calculates the nebular Lyα radiation does not predict the intense Lyα radiation that is needed to explain the presence of strong pumped Fe II lines. It is possible that Lyα line has an origin other than just the nebula condition. Thus, there may be a strong stellar Lyα emission. Indeed, the strong stellar P Cygni Balmer lines with widths of $\pm$1000 km s^{-1} imply a corresponding strong intrinsic stellar Lyα emission. In addition, η Carinae is known as a massive star with strong wind a mass-loss rate of $\approx 10^{-3}\ M_\odot$ yr^{-1} (Davidson et al. 1995; Hillier et al. 2001). The wind speed of $\geq$300 km s^{-1} can easily produce a P Cygni profile with a strong redshifted emission of the Lyα profile, and could explain the effectiveness of Lyα pumping at $\sim$1218 Å.

We have changed the Lyα intensity from model A to model B to reproduce the intensities of observed primary cascades. There are three main sources of uncertainties for the Lyα pumping models: the strength of Lyα, the shape of the Lyα profile, and the A values of Fe II transitions. We have demonstrated that model predictions depend on the accuracy of the A values, which determine the radiative rates. All pumped channels use theoretical transition probabilities. Experimental or better theoretical A values will most likely improve model predictions.

The major factors for the efficiency of the pumping are the Lyα intensity, the Fe II transitions coincidence with Lyα wavelength, and the Fe II transition probabilities. Pumping by a blackbody radiation field works more effectively than Lyα fluorescence in BD blobs. Only 24 strong features from more then 200 Fe II lines and blends are due to Lyα fluorescence. Even in the case of strong Lyα radiation, the effects of continuum pumping are more important for the shape of the Fe II emission spectrum.

If the Lyα radiation comes from spatially extended region of the disc, the total Lyα pumping effects will be much stronger than that produced by Lyα of nebula or central source origin. The increased Lyα intensity is modeled by increasing the number of photons in order to reproduce the strength of

observed Fe II lines. The total contribution of Lyα pumping to the origin of Fe II emission is weaker than that of the blackbody radiation.

9. IMPACT OF ATOMIC DATA ACCURACY ON THE Fe II EMISSION MODELS

The modeling of the Fe^+ ion requires an enormous amount of atomic data. In particular, energy levels, A values, and collisional excitation rates are needed to predict the Fe II emission.

The atomic data are not always known with the required accuracy, and in some cases there are no data available. These limitations affect our models. All wavelengths are based on experimental data, whereas all excitation rates are theoretical, as are the A values for forbidden lines. The A values given for the allowed transitions vary depending on what database is used. In the IRON project (Nahar 1995), all A values are theoretical, but in the Kurucz database (1981), experimental A values are inserted where available.

The main discrepancies between our model and observations that can be attributed to atomic data are due to the following reasons:

1. A values are not known at all for many semiforbidden transitions. For these we have inserted reasonable estimates.

2. Theoretical A values for allowed transitions are calculated in the LS-coupling approximation (Nahar 1995). The deviation from LS coupling is stronger for the upper Fe II levels (Johansson 1984). The close energy spacing of the upper levels leads to their mixing.

3. Collisional excitation rates are calculated only for transitions between the lowest 64 levels (Bautista, Peng, & Pradhan 1996). For other observed lines we used the less accurate g-bar approximation.

As an example of strong mixing, we discuss the famous Fe II $\lambda\lambda$2507, 2509. They originate from upper levels that are very close to each other at 90067.347 ($^6F^o_{9/2}$) and 90042.779 ($^4G^o_{9/2}$) cm^{-1}, and they both cascade to the same lower level at 50187.813 cm^{-1} ($c\,^4F_{7/2}$). The values for pumping and primary cascades derived from LS-coupling calculations are so small (Table 2) that when they are used in calculations, neither line is predicted to be strong. When we add mixing (§ 8), Fe II $\lambda\lambda$2507 and 2509 lines become the strongest lines in the whole Fe II spectrum, a factor of 3 stronger than other Fe II lines.

We have performed calculations for Lyα pumping using the different atomic data sets (§ 8). Model B includes Nahar (1995) data, and model C includes Kurucz (1981) data for the important pumping routes and primary cascades due to Lyα. The A values differ by up to a factor of 100. Comparison of models B and C (Figs. 17 and 18) demonstrates the importance of accurate A values for the model. The Kurucz data used for model C predict the presence of observed pumped levels better than calculations with Nahar's data. In addition, the model spectrum based upon the Kurucz data set predicts more Fe II emission lines between 9000 and 9700 Å pumped by Lyα, which is more consistent with observations. This suggests that the accuracy of atomic data must be improved.

The narrow and strong Fe II lines of the BD blobs allow us to compare in great detail model predictions with observations. Further calculations and/or measurements for the unknown A values should improve model predictions.

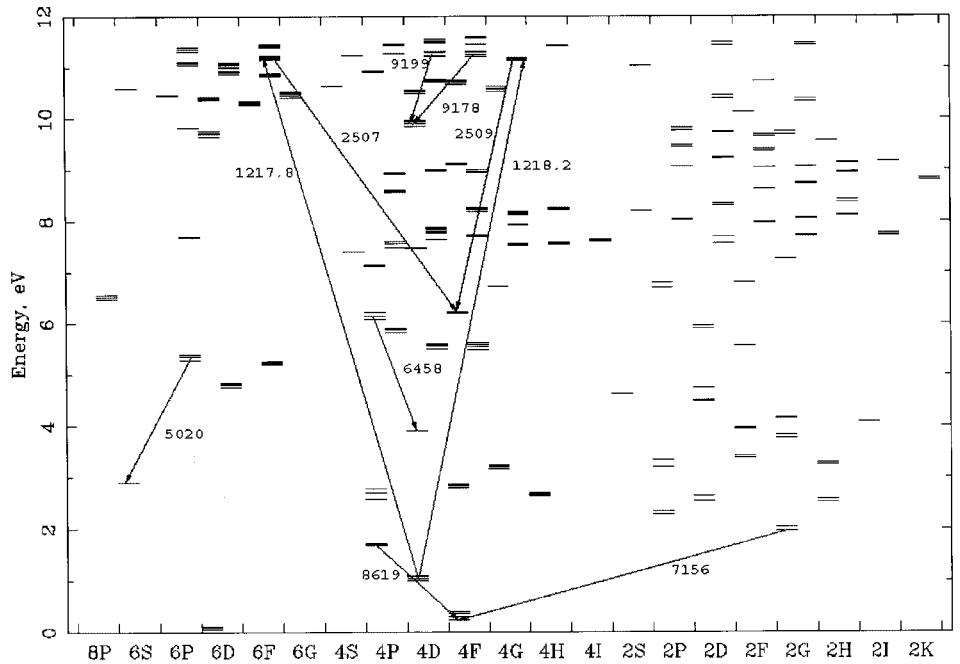

FIG. 18.—A few Fe II and [Fe II] lines originated due to different excitation conditions, shown in energy diagram. Collisional excitation and continuum pumping are responsible for the origin lines below 2 eV (e.g., 7156 and 8619 Å). Lines below 6 eV are pumped by continuum (e.g., 5020 and 6458 Å). Lyα pumping results the Fe II primary cascades observed in UV (e.g., 2507 and 2509 Å) and near IR (e.g., 9178 and 9199 Å). Verner et al. (2000) discussed in detail the main continuum-pumping channels. They start from a^4F term. The main Lyα-pumping channels (e.g., 1217.8 and 1218.2) work effectively from a^4D term and populate levels up to 11 eV.

10. SUMMARY

The BD blob spectrum of η Carinae is uniquely rich in Fe II and [Fe II] lines. The Fe II studies reveal details of physical conditions in the emitting region, and indicate shortcomings in the atomic data for Fe^+ ion.

We conclude that Fe II and [Fe II] lines in the BD blob spectrum are due to the dominant excitation mechanisms (Fig. 18):

1. Pumping by the blackbody-like stellar radiation field from the central source of η Carinae produces the strong and rich spectrum in the 4000–6500 Å range. Most of observable [Fe II] and Fe II lines have accurate A values (Quinet et al. 1996). These lines are in a good agreement with model predictions.

2. Primary cascades after Lyα fluorescence are responsible for 24 strong Fe II lines in the 8000–10000 Å range and in particular Fe II $\lambda\lambda$2507, 2509 in the BD blobs. Secondary cascades have much weaker effects. However, they contribute to the strengths of many other Fe II emission lines. We have postulated a large Lyα flux along with a broad emission profile to explain the observed Fe II primary cascades. In our future work we will study Lyα pumping in greater detail. The Fe II level mixing, the number of Fe II channels involved in excitation, the Lyα intensity, and the profile width and shape are the most important unknown factors.

3. Collisional excitation dominates in the formation of strong [Fe II] lines in the 7000–9000 Å range. For $n_e = 10^5$–10^7 cm^{-3}, the lowest levels of Fe^+ can be populated by collisions. The strength of the [Fe II] λ7156 is systematically underpredicted for a constant-density model. It is not clear if its intensity is due to lower density component (B or D), uncertainties in atomic data, or geometric effects. Small collisional strengths or an overlooked excitation route might also affect the predicted intensity.

We have used the Fe II spectrum to derive physical conditions in the BD blobs. The best fit to the observed spectrum is achieved in the 4000–6000 Å range at constant density $n_e \sim 10^6$ cm^{-3} and $T_{BB} \sim 15{,}000$ K. The dominant Fe^+ ionization fraction and rich Fe II spectrum suggest the electron temperature range of $T_e = 5000$–7500 K. Our model predicts that the Fe^+/Fe^{2+} has very sharp transition due to collisional ionization at $\sim 10^6$ cm^{-3} and the size of blob $\approx 10^{15}$ cm^{-3}. The Fe ionization structure, low electron temperature in plasma, the shape of blackbody radiation, and intense Lyα radiation provide conditions favorable for a rich Fe II spectrum. Blackbody radiation and Lyα pumping are the main excitation mechanisms for the Fe II ion in the BD blobs.

As our first step, we have focused on Fe II emission analysis of the spectrum of the BD blobs from 1998 observations. Extensive *HST*/STIS η Carinae observations at different positions and during other epochs are available. The morphology of the Homunculus Nebula surrounding η Carinae is very complex. Line profile analysis by Viotti et al. (1989) and Davidson et al. (1995) suggests a wider range of velocities than expected from spherical geometry. In addition, an inhomogeneous dust distribution may selectively obscure the radiation field. As a result, any of the combinations considered above (e.g., collisions, blackbody radiation) may be responsible for the Fe II and [Fe II] emission spectrum at other than BD positions.

For the first time, we have used detailed non-LTE Fe II models to bracket physical parameters of Fe^+-rich plasma in the BD blobs of η Carinae. Most of the [Fe II] and Fe II lines predicted by our model are in a good agreement with observations.

E. V.'s research on η Carinae at NASA GSFC and the CUA is supported by STIS GTO resources. E. V. is grateful to J. Hillier for the discussion of different aspects of photoionization modeling on the central star. We thank G. Ferland for adding a high-resolution option to the CLOUDY code to treat more accurately line-pumping processes. We give special thanks to Keith Feggans, Don Lindler, and Terry Beck for their computational and data-reduction support.

REFERENCES

Baldwin, J., Verner, E., Verner, D., Ferland, G., Martin, P., Korista, K., & Rubin, R. 2000, ApJS, 129, 229
Bautista, M. A., Peng, J., & Pradhan, A. K. 1996, ApJ, 460, 372
Damineli, A., Conti, P. S., & Lopes, D. F. 1997, NewA, 2, 107
Damineli, A., Stahl, O., Kaufer, A., Wolf, B., Quast, G., & Lopes, D. F. 1998, A&AS, 133, 299
Davidson, K. 1999, in ASP Conf. Ser. 179, η Carinae at the Millennium, ed. J. A. Morse, R. M. Humphreys, & A. Damineli (San Francisco: ASP), 6
Davidson, K., Ebbets, D., Weigelt, G., Humphreys, R. M., Hajian, A. R., Walborn, N. R., & Rosa, M. 1995, AJ, 109, 1784
Davidson, K., & Humphreys, R. M. 1997, ARA&A, 35, 1
Davidson, K., et al. 1997, AJ, 113, 335
Ebbets, D. C., Walborn, N. R., & Parker, J. W. 1997, ApJ, 489, L161
Ferland, G. 1996, Hazy: a Brief Introduction to CLOUDY (Lexington: Univ. Kentucky Int. Rep.)
Ferland, G. J., Korista, K. T., Verner, D. A., Ferguson, J. W., Kingdon, J. B., & Verner, E. M. 1998, PASP, 110, 761
Fuhr, J. R., Martin, G. A., & Weise, W. L. 1988, J. Phys. Chem. Ref. Data Suppl., 17, 4
Gull, T., Ishibashi, K., & Davidson, K. 1999, in ASP Conf. Ser. 179, η Cariane at the Millennium, ed. J. A. Morse, R. M. Humphreys, & A. Damineli (San Francisco: ASP), 144
Gull , T., Ishibashi, K., Davidson, K., & Collins N. 2001, in ASP Conf. Ser. 242, η Carinae and Other Mysterious Stars, ed. T. Gull, S. Johansson, & K. Davidson (San Francisco: ASP), 391
Hamann, F., Davidson, K., Ishibashi, K., & Gull, T. 1999, in ASP Conf. Ser. 179, η Carinae at the Millennium, ed. J. A. Morse, R. M. Humphreys, & A. Damineli (San Francisco: ASP), 116
Hartman, H., & Johansson, S. 2000, A&A, 359, 627
Hillier, D. J., Crowther, P. A., Najarro, F., & Fullerton, A. W. 1998, A&A, 340, 483
Hillier, D. J., Davidson, K., Ishibashi, K., & Gull, T. 2001, ApJ, 553, 837
Ishibashi, K., et al. 1999, ApJ, 524, 983
Johansson, S. 1984, Phys. Scr., T8, 63
Johansson, S., & Hamann, F. 1993, Phys. Scr., 47, 157
Johansson, S., & Jordan, C. 1984, MNRAS, 210, 239
Johansson, S., & Letokhov, V. 2001, A&A, 378, 266
Kurucz, R. L. 1981, Semiempirical Calculation of *gf* Values, IV: Fe II (SAO Special Rep. 390; Washington: SAO)
Mewe, R. 1972, A&A, 20, 215
Nahar, S. N. 1995, A&A, 293, 967
Osterbrock, D. E. 1989, Astrophysics of Gaseous Nebulae and Active Galactic Nuclei (Mill Valley: University Science Books)
Pittard, J. M., & Corcoran, M. F. 2002, A&A, 383, 636
Pradhan, A. K., & Peng, J. 1995, in The Analysis of Emission Lines, ed. R. Williams & M. Livio (Cambridge: Cambridge Univ. Press), 8
Quinet, P., Le Dourneuf, M., & Zeippen, C. J. 1996, A&AS, 120, 361
Verner, D., & Yakovlev, D. 1986, Ap&SS, 165, 27
Verner, E. M., Verner, D. A., Baldwin, J., Ferland, G., & Martin P. 2000, ApJ, 543, 831
Verner, E. M., Verner, D. A., Korista, K. T., Ferguson, J. W., Hamann, F., & Ferland, G. J. 1999, ApJS, 120, 101
Viotti, R., Rossi, L., Cassatella, A., Altamore, A., & Baratta, G. 1989, ApJS, 71, 983
Weigelt, G., & Ebersberger, J. 1986, A&A, 163, L5
Zethson, T. 2001, Ph.D. thesis, Univ. Lund
Zhang, H. L., & Pradhan, A. K. 1995, A&A, 293, 953